

Supporting Information

Suppressing Migration of Ru in High-Entropy Alloy for Durable Acidic Oxygen Evolution

Le Su^a, Xiaokang Chen^b, Yi Tan^b, Wei-Qiao Deng^b, Hao Wu^{b,c*}, Xiangyang Miao^{a*}

^a College of Physics and Information Engineering, Shanxi Normal University, No.339

Taiyu road, Xiaodian District, Taiyuan 030031, China.

^b Institute of Frontier Chemistry, School of Chemistry and Chemical Engineering,

Shandong University, Qingdao, Shandong 266237, China.

^c Suzhou Research Institute, Shandong University, Suzhou, Jiangsu 215123, China.

Characterization

X-ray diffraction (XRD) patterns were obtained by X-ray diffractometer (Bruker D8-Advance) equipped with a Cu K α radiation source ($\lambda = 1.5418 \text{ \AA}$) to record the crystal diffraction patterns of samples. The morphology and structure of all samples were characterized by field-emission scanning electron microscopy (FE-SEM, Hitachi, SU-8010) and high-resolution transmission electron microscopy (HR-TEM, JEM-2100, 200 kV) with X-ray energy-dispersive spectroscopy. The inductively coupled plasma emission spectrometer (ICP-MS Agilent-720) analysis was conducted to analyze the elemental content in the samples. The surface composition and valence state of the samples were characterized by X-ray photoelectron spectroscopy (XPS, Kratos Axis Ultra DLD).

Electrochemical measurements

All electrochemical data tests were achieved by CHI 760E electrochemical workstation (CH Instruments, China) with a three-electrode system in an O₂ saturated 0.5 M H₂SO₄. The as-prepared samples supported on carbon paper, a mercury oxide electrode (Ag/AgCl) and a carbon rod (4 mm in diameter) were employed as the working, reference and counter electrode, respectively. All the potentials with regard to Ag/AgCl were calibrated to the reversible hydrogen electrode (RHE) according to the following equation: $E(\text{RHE}) = E(\text{vs. Ag/AgCl}) + 0.059 \times \text{pH} + 0.197$. All the measurements above were corrected by manual IR compensation using the current and the solution resistance. Furthermore, all experiments were repeated at least three times to ensure reliability and reproducibility. Cyclic Voltammetry (CV)

measurements for OER were scanned in the potential range from 1 to 2 V (vs. Ag/AgCl) at a scanning rate of 200 mV·s⁻¹. And the corresponding polarization curves were obtained by using Linear Sweep Voltammetry (LSV) with a scan rate of 5 mV·s⁻¹, respectively. The stability test was implemented using chronopotentiometric method at certain potentials. The electrochemical data were not collected until the signals of working electrodes stabilized after scanning several times. Electrochemical impedance spectroscopy (EIS) experiments were conducted in the frequency range from 100 KHz to 1 Hz with an amplitude potential of 5 mV.

The S-number is calculated by the following equation:

$$S - number = \frac{n(O_2)}{n_{leached\ metal}}$$

where n(O₂) (μmol) in equation represents the number of moles of O₂ during OER electrolysis, and n_{leached metal} (μmol) represents the number of leached active metals in the electrolyte at a certain time. The amounts of dissolved metal were extracted from the ICP-MS results.

HEAs parameter calculation

The contribution of the mixed configuration entropy can be obtained through equation:

$$\Delta S_{mix} = -R \sum_{i=1}^n C_i \ln C_i$$

where R is the molar gas constant (8.314 J K⁻¹ mol⁻¹), C_i represents the molar fraction of the element component, n represents the number of elements in the alloy.

In general, HEAs can be characterized as an alloy that contains at least five elements with ΔS_{mix} greater than 1.5 R.

To describe the comprehensive effect of the atomic size difference in n-element contained alloy, the parameter δ can be expressed as follows equation:

$$\bar{r} = \sum_{i=1}^n C_i r_i$$

$$\delta = \sqrt{\sum_i C_i \left(1 - \frac{r_i}{\bar{r}}\right)^2}$$

Where C_i is the atomic percentage of the i^{th} component, r_i is the atomic radius, and δ is the mean square deviation of the atomic size of elements. It can be found that the large atomic size difference will cause serious lattice distortion and thus result in the increase of free energy in alloy, which leads to poor stability of solid solution.

The valence electron concentration (VEC) of the solid solution determines the crystalline phase exhibited by high-entropy alloys. It can be obtained through equation:

$$VEC = \sum_{i=1}^n C_i (VEC)_i$$

In the above equations, C_i represents the atomic percentage of the i^{th} component, $(VEC)_i$ is the valence electron concentration of the i^{th} element.

Calculation for turnover frequency (TOF)

The turnover frequency (TOF) of the HEA/PANI-CP electrocatalyst was calculated based on the assumption that each Ru atom in the catalyst constitutes an active center.

The number of Ru atoms was determined through a two-step quantification process:

First, the Ru mass loading (0.15 mg cm^{-2}) was experimentally measured through inductively coupled plasma (ICP) analysis, which revealed a Ru content of 4.6 at% in the composite catalyst. Subsequently, the molar quantity of Ru atoms was calculated

using the element's molar mass (101.07 g mol⁻¹). These parameters were then incorporated into the standard TOF calculation equation to determine the catalytic efficiency of the system.

$$TOF(O_2 s^{-1}) = \frac{\text{Total } O_2 \text{ turnovers per geometric area}}{\text{Active sites per geometric area}}$$

The number of total O₂ turnovers per geometric area was calculated from the current density (J) for the OER-LSV polarization:

$$\begin{aligned} &= \left(\frac{|J| mA}{cm^2} \right) \left(\frac{1 C/s}{1000 mA} \right) \left(\frac{1 mol}{96453.8 C} \right) \left(\frac{1 mol}{4 e} \right) \left(\frac{6.023 \times 10^{23}}{1 mol O_2} \right) \\ &= 1.56 \times 10^{15} \frac{O_2/s}{cm^2} \text{ per } \frac{mA}{cm^2} \end{aligned}$$

The upper limit of active sites density for HEA/PANI-CP:

$$\begin{aligned} &= \frac{0.15 mg cm^{-2} \times 10^{-3} \times 4.6 \% \times 6.023 \times 10^{23}}{101.07 g mol^{-1}} \\ &= 4.11 \times 10^{16} Ru \text{ site per } cm^2 \end{aligned}$$

Finally, the TOF of HEA/PANI-CP can be obtained via the current density from the OER-LSV polarization curves and according to:

$$TOF = \frac{1.56 \times 10^{15}}{4.11 \times 10^{16}} \times |J| = 0.038|J|$$

Particularly, at the overpotential of 258 and 422 mV, the current density of OER are 10 and 100 mA cm⁻², respectively. Therefore, the TOF values of HEA/PANI-CP electrocatalyst were calculated to be:

$$TOF_{(258 mV)} = 0.038 \times 10 = 0.38 O_2 s^{-1}$$

$$TOF_{(422 mV)} = 0.038 \times 100 = 3.8 O_2 s^{-1}$$

DFT calculations

The Vienna Ab-initio Simulation Package (VASP) was employed to conduct all Density Functional Theory (DFT) calculations.¹⁻² The Perdew-Burke-Ernzerhof (PBE) exchange-correlation functional, employing the generalized gradient approximation (GGA) method, was utilized in this study.³⁻⁴ The projected augmented wave (PAW) method was utilized to describe core-valence interactions in all DFT calculations.⁵ The energy cutoff for plane wave expansions was set to 450 eV, and the $2 \times 2 \times 1$ Monkhorst-Pack grid k-points were used to sample the Brillouin zone integration for structural optimization. A 10 Å vacuum was applied the model to eliminate image interactions. Structural optimization was carried out with energy and force convergence criteria setting at 1.0×10^{-5} eV and 0.02 eV \AA^{-1} , respectively. Climbing image nudged elastic band (CI-NEB) is applied to find the transition states of Na diffusion.

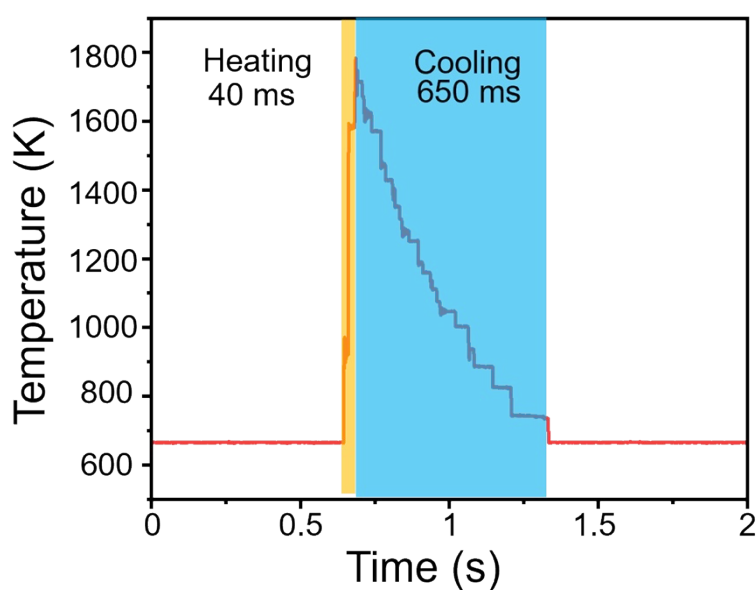


Fig. S1 Temperature rise and fall processes during the thermal shock.

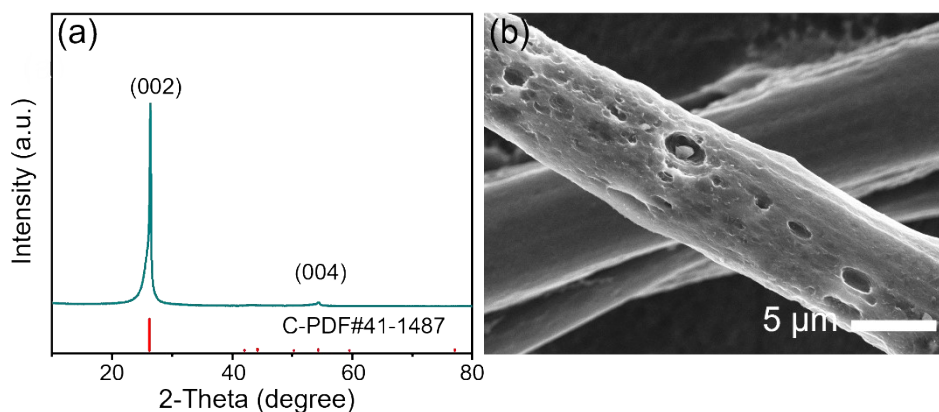


Fig. S2 Representative XRD and SEM image of PANI-CP.

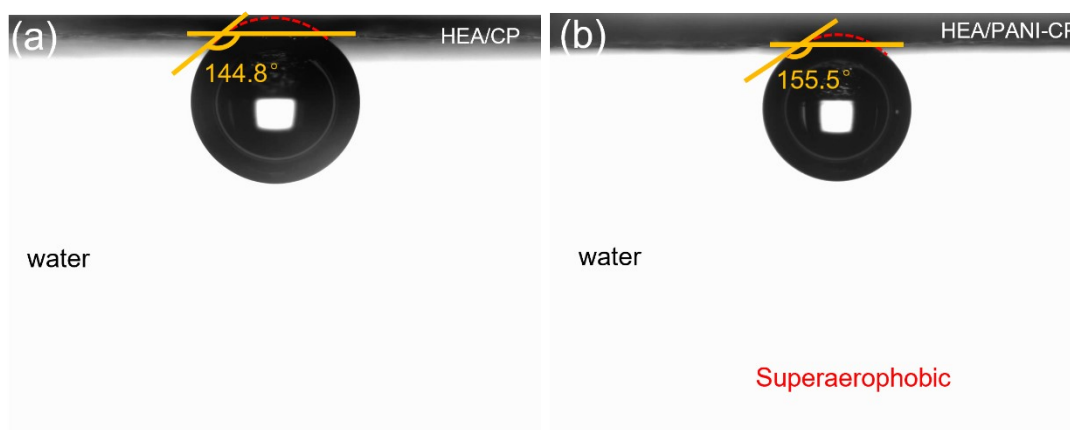


Fig. S3 Bubble contact angles of (a) HEA/CP and (b) HEA/PANI-CP.

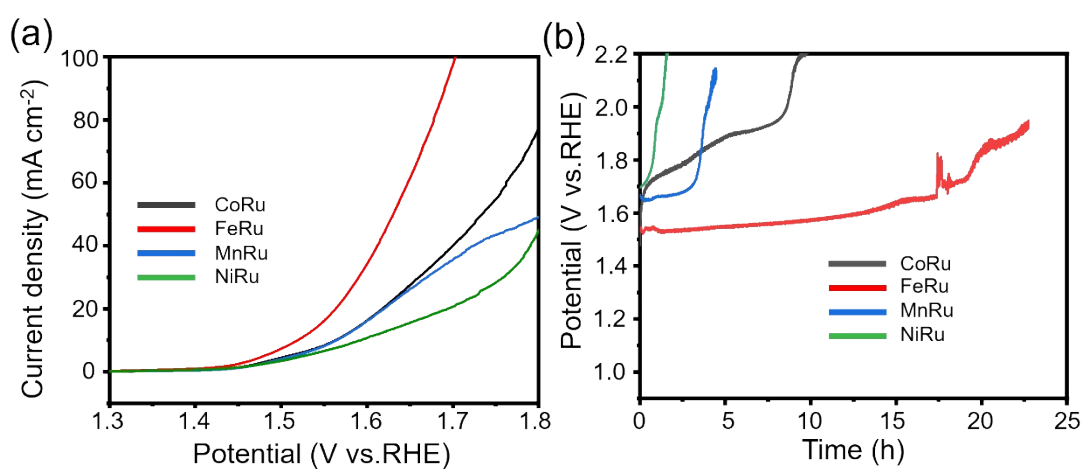


Fig. S4 (a) LSV curves of different binary alloys. (b) The long-term durability measurement of different binary alloys.

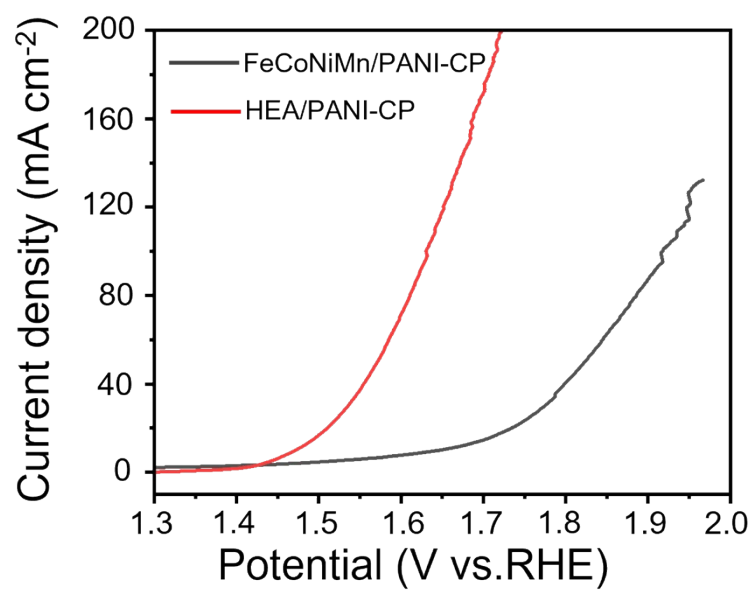


Fig. S5 LSV curves of HEA/PANI-CP and FeCoNiMn/PANI-CP.

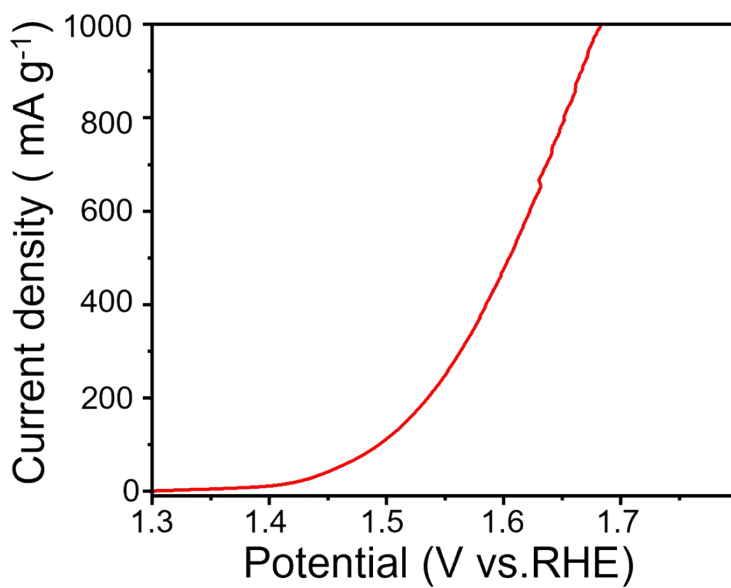


Fig. S6 Mass normalized LSV curves of the HEA/PANI-CP.

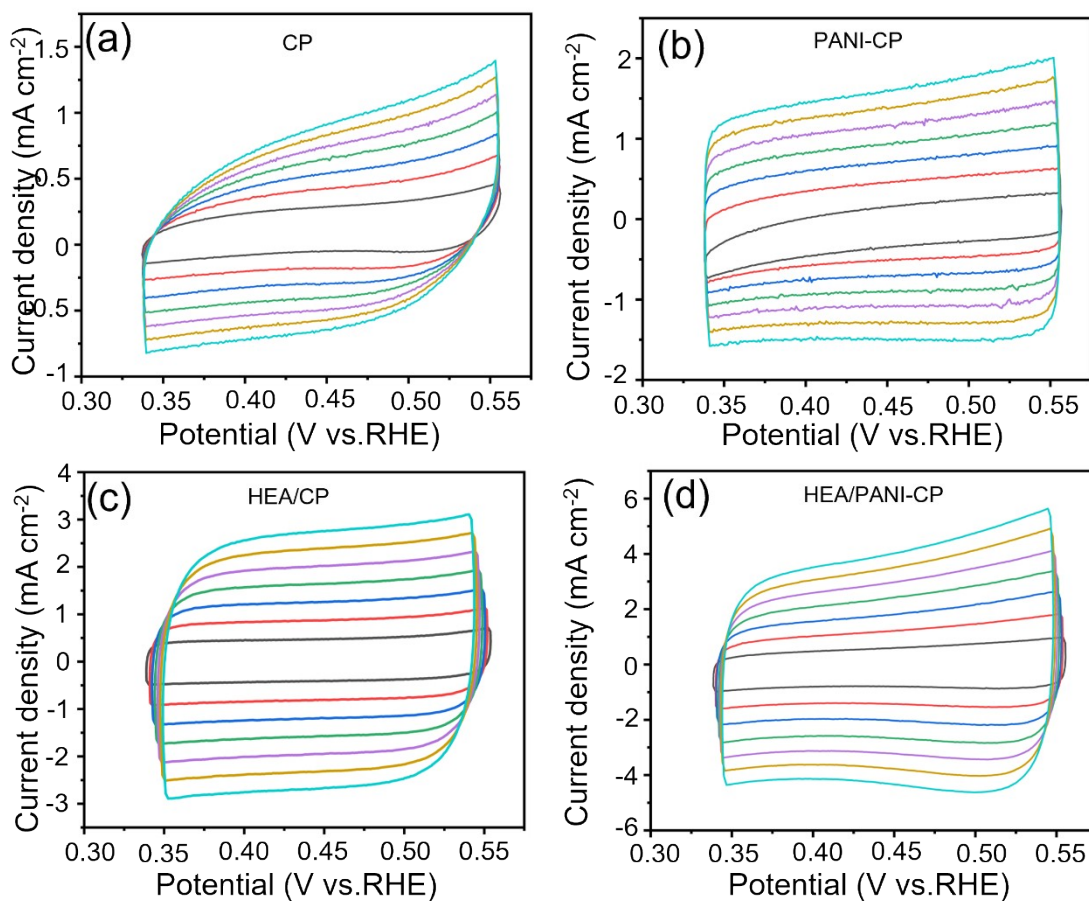


Fig. S7 CV curves of (a) CP, (b) PANI-CP, (c) HEA/CP, (d) HEA/PANI-CP in the non-faradaic region with different scanning rates from 20 to 140 mV s^{-1} .

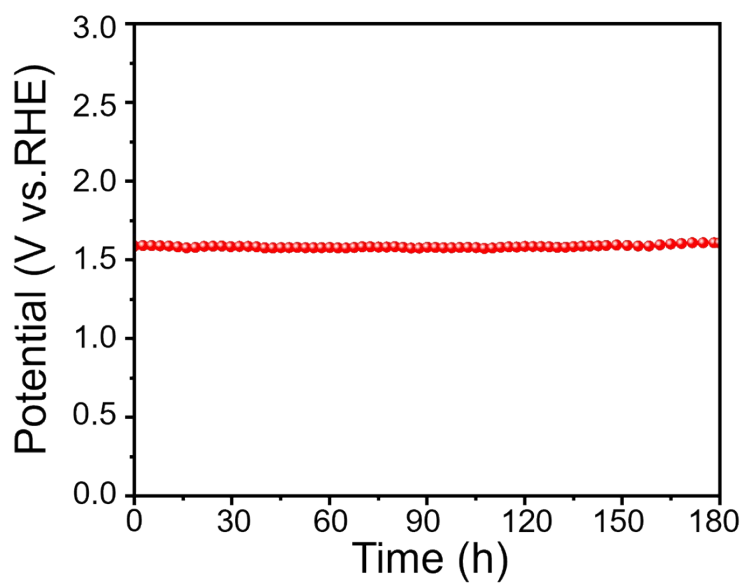


Fig. S8 The long-term durability measurement of HEA/PANI-CP at 100 mA cm^{-2} .

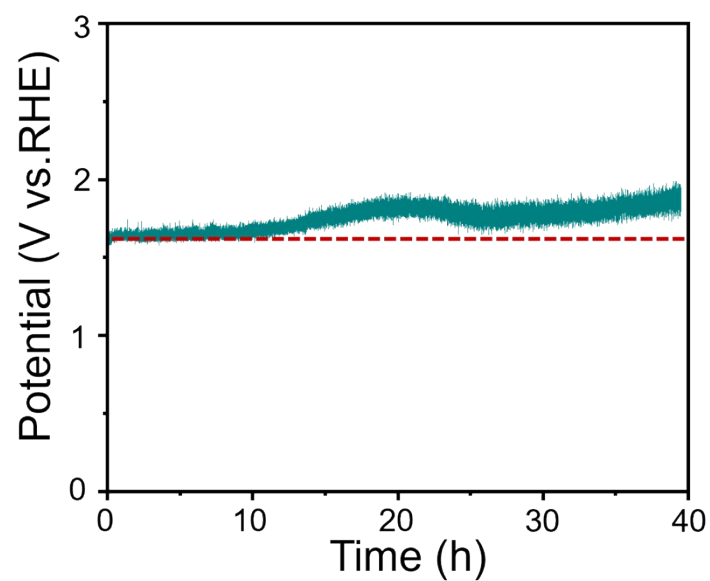


Fig. S9 The long-term durability measurement of HEA/ CP.

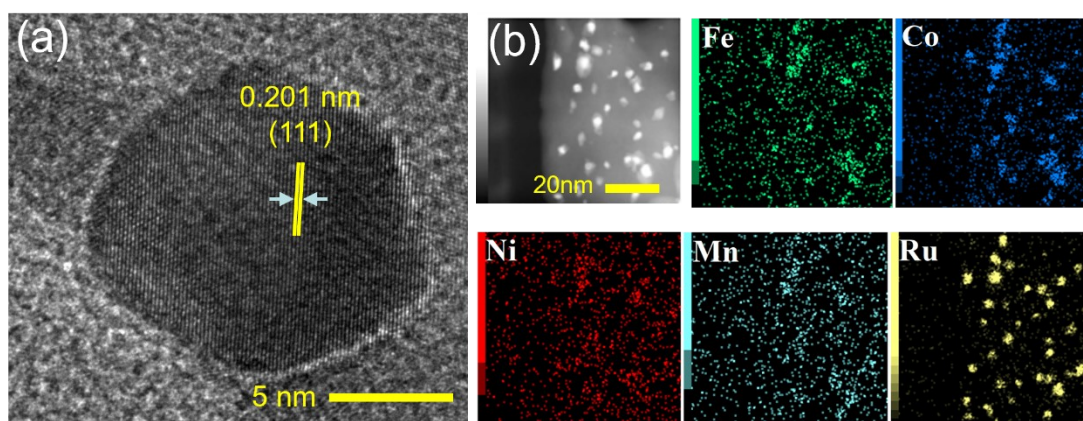


Fig. S10 HRTEM image (a) and EDS elemental mapping (b) of the HEA/PANI-CP catalyst after continuous 180 h at 100 mA cm⁻² for OER.

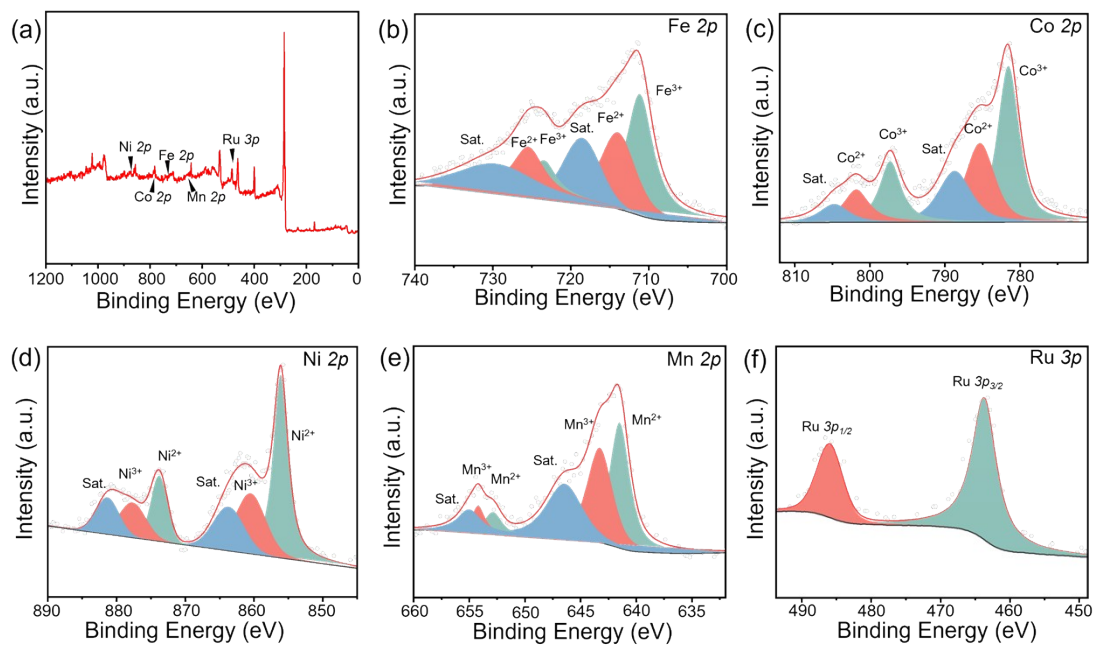


Fig. S11 (a) XPS full survey spectrum of HEA/PANI-CP after continuous OER electrolysis. High-resolution XPS spectra of (b) Fe 2*p*, (c) Co 2*p*, (d) Ni 2*p*, (e) Mn 2*p* and (f) Ru 3*p*.

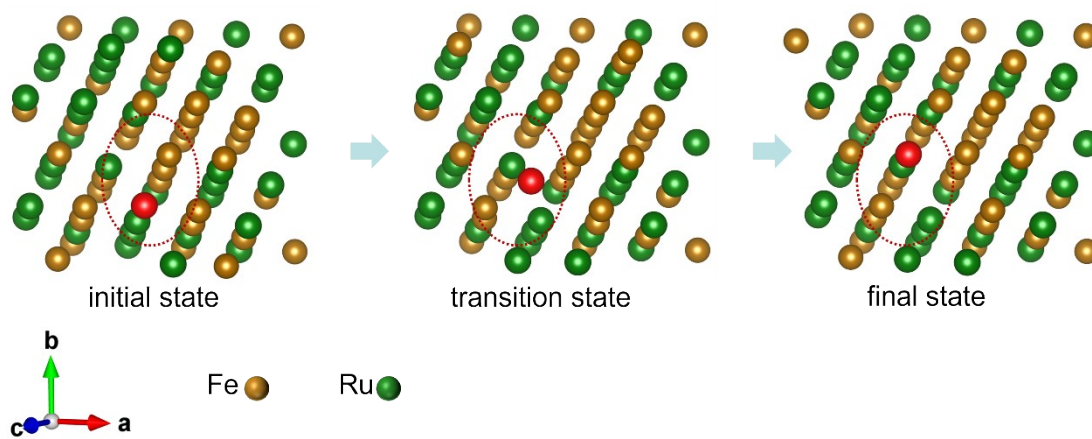


Fig. S12 Migration path of Ru atoms in FeRu.

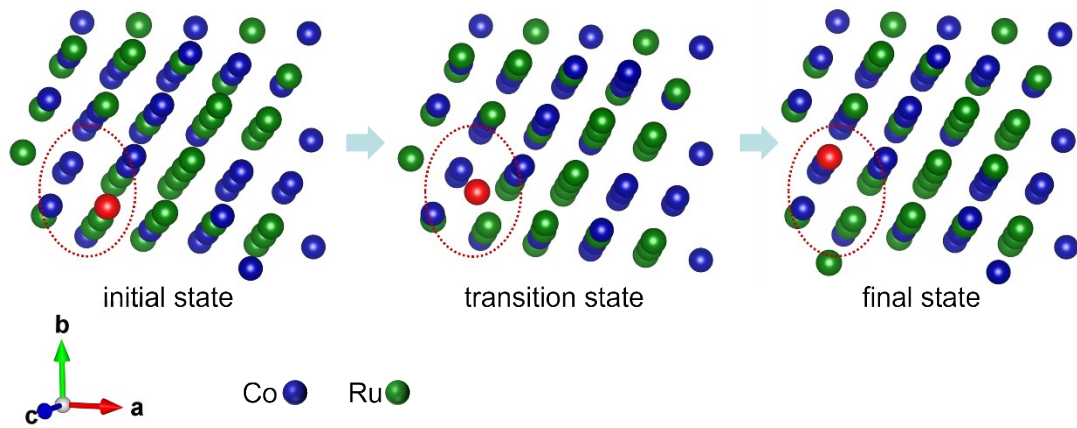


Fig. S13 Migration path of Ru atoms in CoRu.

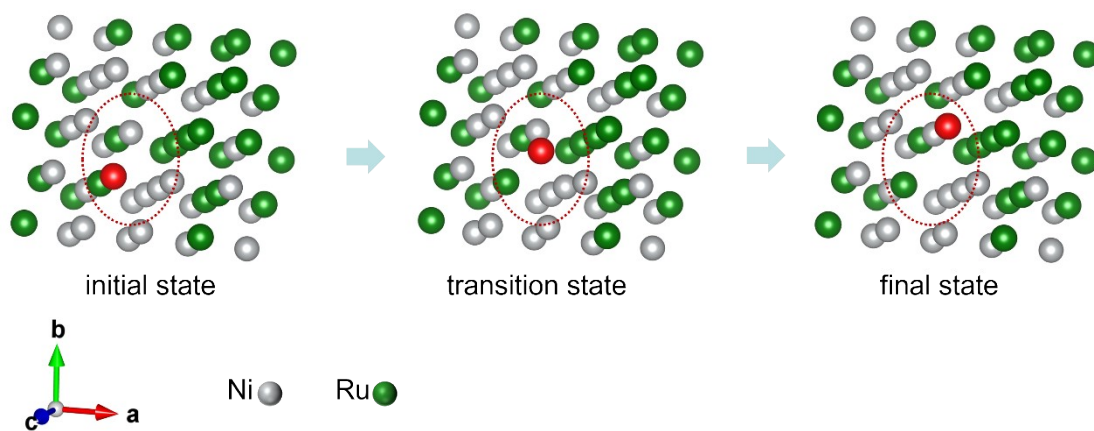


Fig. S14 Migration path of Ru atoms in NiRu.

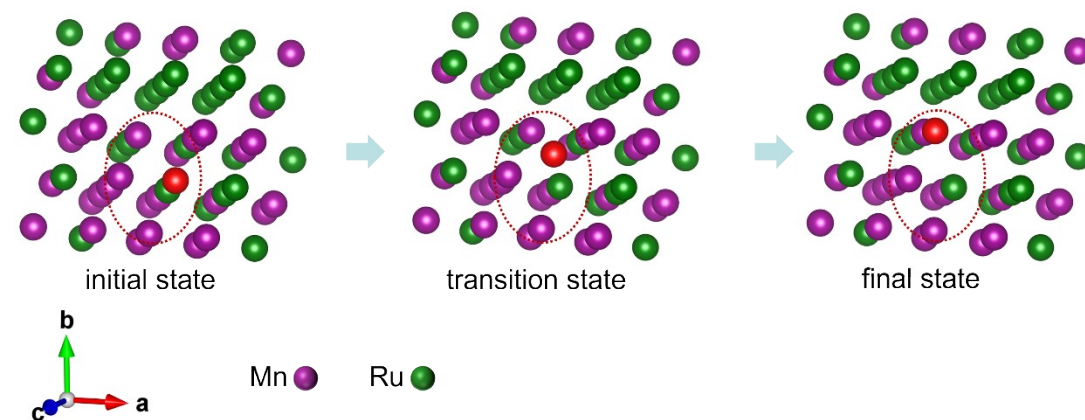


Fig. S15 Migration path of Ru atoms in MnRu.

Table 1 Chemical compositions of the synthesized catalysts measured by ICP.

Fe		Co		Ni		Mn		Ru	
atom %	wt %								
6.06	3.38	4.49	2.64	5.58	3.27	5.81	3.21	4.60	4.65

Table 2 Chemical compositions of the synthesized catalysts measured by ICP after 24h stability test.

	HEA	FeRu	CoRu	NiRu	MnRu
Fe	1.8434	0.2092			
Co	2.5737		1.5272		
Ni	3.2114			3.1237	
Mn	1.7535				0.3708
Ru	2.4837	52.698	8.4449	7.9175	14.603

Table 3 Comparison of OER catalytic performance of HEA/PANI-CP with other recently reported electrocatalysts in 0.5 M H₂SO₄ solution.

Sample	Overpotential (mV)	Stability (h)	Reference
	@ 10mAcm ⁻²	@ 10mAcm ⁻²	
HEA/PANI-CP	258	300	This work
Ni-RuO ₂	214	200	Nat. Mater. 2023, 22, 100.
Pr ₃ Ir _{1-x} Mo _x O ₇	259	200	Nat. Commun. 2023, 14, 4127.
Y ₂ MnRuO ₇	270	40	Nat. Commun. 2023, 14, 2010.
IrO ₂ @TaB ₂	288	120	Nat. Commun. 2023, 14, 5119.
Ir _{0.06} Co _{2.94} O ₄	290	200	J. Am. Chem. Soc. 2021, 143, 5201.
Ti-IrO _x /Ir	254	100	Chem, 2023, 9, 2931-42.
Ir/WO ₃ /CC	249	35	Angew. Chem. Int. Ed. 2024, 63, e202406947.
RuO ₂ -WC	347	10	Angew. Chem. Int. Ed. 2022, 61, e202202519.
H-Ti@IrO _x	277		J. Mater. Chem. A, 2020, 8, 24743 – 24751.
HP-RuO _x	237	140	J. Mater. Chem. A, 2025, 13, 312–324.

References

- [1] G. Kresse, J. Hafner, *Phys. Rev. B*, 1993, **47**, 558-561.
- [2] G. Kresse, J. Hafner, *Phys. Rev. B*, 1994, **49**, 14251-14269.
- [3] J. P. Perdew, K. Burke, *Phys. Rev. Lett.*, 1996, **77**, 3865-3868.
- [4] G. Kresse, D. Joubert, *Phys. Rev. B*, 1999, **59**, 1758-1775.
- [5] P. E. Blöchl, *Phys. Rev. B*, 1994, **50**, 17953-17979.